Eur. Phys. J. D **2**, 273–278 (1998)

THE EUROPEAN PHYSICAL JOURNAL D

The evolution of electronic structure in lanthanide metal clusters: Threshold photoionization spectra of Ce_n and Pr_n

G.M. Koretsky and M.B. Knickelbein[a]

Chemistry Division, Argonne National Laboratory, Argonne, IL 60439, USA

Received: 2 January 1998 / Accepted: 10 March 1998

Abstract. The photoionization spectra of Pr_2-Pr_{21} and Ce_2-Ce_{17} have been measured near threshold. The ionization potentials (IPs) of Pr_n and Ce_n vary discontinuously with size, but trend downward toward the work function of the bulk metals. In general, the IPs of cerium clusters display more variation than those of praseodymium clusters. The sudden discontinuities observed in the IPs of both Ce_n and Pr_n is akin to that displayed by clusters of transition metal atoms, suggesting that as in transition metal clusters, the rapid evolution in geometric structure with size is the source of these discontinuities.

PACS. 36.40.-c Atomic and molecular clusters – 33.20.Lg Ultraviolet spectra – 33.80.Eh Autoionization, photoionization, and photodetachment

1 Introduction

It is well known that the valence electronic structures of most lanthanide elements differ in their atomic forms from those of the corresponding bulk metal [1]. Specifically, for elements 59-62 [Pr, Nd, Pm, and Sm] and 65-69 [Tb, Dy, Ho, Er, and Tm], the atoms are divalent, $4f^n\ 6s^2$, whereas the corresponding infinite solids display *trivalent* electronic band structure, $4f^{n-1}\ (5d,\ 6s)^3$. In contrast, the remainder of the lanthanides display invariant valence behavior: Ce, Gd, and Lu are trivalent for both atom and bulk, while Eu and Yb are divalent in both cases [2]. For those metals exhibiting this divalent-trivalent dichotomy, the crossover in electronic configuration necessarily occurs in some finite size regime–in a cluster or small particle. Identification of the particle size at which this transition occurs has been the subject of several studies. The first experimental studies examined small particles deposited in rare gas matrices [3–6] or on various substrates [7,8]. Niemann *et al.* [3–5] measured the L_{III} x-ray absorption near edge structure (XANES) of Pr_n, Nd_n, and Sm_n deposited in solid matrices of Ar, Ne, and Kr. In these studies, a gradual evolution of the x-ray absorption spectra from atomic to bulk behavior was observed as the particle size was varied. Specifically, at certain matrix loadings, two peaks were seen in the LIII XANES spectra, one assigned to the $2p_{3/2} \rightarrow 5d$ transition in these small divalent lanthanide metal particles and the second corresponding to the same transition in the larger trivalent particles, approximately 5−8 eV higher in energy. It was determined that the valence transition occurred for clusters containing approximately 5 atoms for praseodymium and neodymium and around 13 atoms for samarium. Blancard *et al.* found similar results for Tl particles grown in rare gas matrices [6]. However, in each of these matrix studies, the precise size at which the transition occurred was masked by the unavoidable distribution of particle sizes produced in the samples. In order to avoid this complication, it becomes necessary to either prepare a monodisperse sample, or to devise an experiment in which the individual particle sizes within a distribution can be selectively studied. Mass spectrometry is one approach that can be adapted to fulfill the latter requirement, but requires preparation of a gas phase sample.

The ability to produce a molecular beam of isolated lanthanide clusters was first demonstrated by Bréchignac and coworkers [9] using the inert gas condensation method. In a subsequent study aimed at understanding the evolution of lanthanide valence electronic structure, that group employed molecular beam photoionization mass spectrometry to determine the effective valences in oxide clusters of Eu, Tm, and Yb as a function of cluster size [10]. An important result of this study was that for Eu_nO_m and Yb_nO_m, oxidized clusters of elements that are normally divalent in both atomic and bulk form, the metals displayed a divalent-to-trivalent transition over the range $n = 2-10$, as determined by an evolution in their m/n ratios. This result underscores the importance of chemical environment in determining the valence state adopted by the lanthanide elements, both in conventional compounds and in small isolated clusters, but leaves the original question unanswered: over which size range does the divalent-to-trivalent transition occur for pure lanthanide elements? In a preliminary effort to better understand the valence electronic behavior of pure lanthanide clusters, we have

[a] e-mail: knickelbein@anlchm.chm.anl.gov

performed near-threshold photoionization spectroscopy studies of isolated cerium and praseodymium clusters. The vertical ionization potentials, reported here for Pr_{2-21} and Ce_{2-17}, are, to our knowledge, the first reported for lanthanide clusters.

2 Experimental Methods

Vertical ionization potentials (IPs) were measured by photoionization mass spectrometry, using a molecular beam apparatus that has been described previously [11]. In brief, cerium or praseodymium atoms were generated by focusing the second harmonic output of a pulsed Nd:YAG laser onto the surface of a target fabricated of the corresponding metal. The cerium target was in the form of a 0.06 cm thick foil (Alfa Aesar, 99.9%) wrapped around a stainless steel rod 0.64 cm in diameter. The praseodymium target was a solid, cylindrical rod 0.64 cm in diameter (Goodfellow, 99.9%). Clusters formed from the vaporized atoms in the midst of helium carrier gas (20 Torr) flowing over the target at approximately 500 std. cm^3 min^{-1} through a flow tube maintained near 70 K. After formation, the clusters resided approximately 10^{-3} s in the flow tube before undergoing a mild supersonic expansion through a 0.1 cm diameter nozzle orifice. The free jet was skimmed into a beam, which passed first into a differential pumping region and then into a detection chamber held at $\sim 10^{-6}$ Torr. Once inside the detection chamber, the molecular beam passed between the ion extraction grids of a time-of-flight (TOF) mass spectrometer. Here, the beam was intersected at 90° by a pulse of tunable ultraviolet laser light, timed to intercept the pulse of clusters as it passed within the ion extraction region. The tunable ultraviolet light was produced by frequency-doubling the output of a pulsed dye laser ($\sim$ 15 ns pulse length). Laser fluences were attenuated to ≤ 200 μJ cm^{-2}, where one-photon photoionization events far exceeded two-photon photoionization and fragmentation events. The mass separated cluster ions were detected using a microchannel plate ion detector. Signal amplification and digitization was performed over 2000 repetitions, and the result was stored in a microcomputer.

For Pr_2−Pr_{12}, ionization potentials were determined from their fluence- normalized photoionization efficiency (PIE) spectra, obtained from the integrated Pr_n^+ mass peaks areas measured at 1 nm intervals. For larger praseodymium clusters, acquisition of high quality PIE spectra was not possible due to significant fluctuations in cluster production, caused by the presence of oxide impurities that were inhomogeneously distributed in the target. In this case, IPs were bracketed by the presence or absence of the corresponding cluster ion mass peaks in TOF spectra recorded at 5 nm intervals.

For the cerium clusters, the fluctuations in cluster production due to the inhomogeneous distribution of oxide impurities in the target were even greater than for the praseodymium clusters. Hence the following normalization procedure was implemented to obtain PIE spectra. Two time-of-flight (TOF) spectra were concurrently recorded on alternate repetitions, one in which the beam was intersected with tunable light from the frequency-doubled output of the dye laser and the second in which the beam was intersected with fixed- frequency light from an ArF laser (6.42 eV). The integrated Ce_n^+ mass peak areas areas from the former TOF spectrum were divided by the integrated Ce_n^+ mass peak areas from the latter TOF spectrum to yield PIE spectra corrected for fluctuations in cluster production.

3 Results

Vertical IPs were assigned from PIE spectra by linearly extrapolating the major post-threshold portion to the baseline of signal. In many cases, the spectra displayed curved "tails" near threshold, attributable to vibrational hot bands [11]. In those cases, the low intensity signal near threshold was not considered when the extrapolation was performed. In other instances, additional linear segments close to threshold were observed and judged to be genuine features of the PIE spectra rather than simply thermal "tails". In such cases that linear portion of the curve lying at lowest energy was extrapolated to baseline to yield the IP. The ±0.05 eV error limits on the assigned IPs reflect the uncertainty of such judgements.

3.1 Praseodymium Clusters

Time-of-flight spectra of praseodymium clusters recorded at three different photoionization wavelengths are shown in Figure 1. Fluence studies were performed in order to determine the range over which the cluster ion signal was dominated by one photon ionization. At photon energies below the one-photon ionization threshold, all cluster ion signal is necessarily due to multiphoton absorption. This is demonstrated for Pr_7 in Figure 2a, where the ion intensity increases with laser fluence F as F^x, $x > 1$. At photon energies above the one-photon ionization threshold, the fluence studies show that at fluences less than or equal to 300 μJ cm^{-2}, the cluster ion intensity increases linearly with photon fluence, thereby demonstrating that multiphoton ionization/fragmentation processes are negligible compared to single photon ionization in this fluence regime. The linear behavior is shown for Pr_7 in Figure 2b.

The production of praseodymium clusters was sufficiently stable to allow measurement of PIE spectra up to Pr_{12}. The PIE spectra of Pr_3, Pr_6 and Pr_{11} are shown in Figure 3. For larger Pr_n clusters, signal fluctuations due to the presence of oxide impurities precluded the acquisition of high quality PIE spectra. For these larger Pr_n cluster, the IPs were bracketed by their presence or absence in TOF spectra recorded at 5 nm photoionization intervals. During the course of the bracketing studies, TOF spectra recorded at 193 nm ($h\nu$ = 6.4 eV) were frequently recorded, in order to verify that bare clusters were being produced in addition to the oxides. The vertical ionization potentials for Pr_2-Pr_{21} are shown in Figure 4a. Although the IPs of Pr_nO_m species were not explicitly measured,

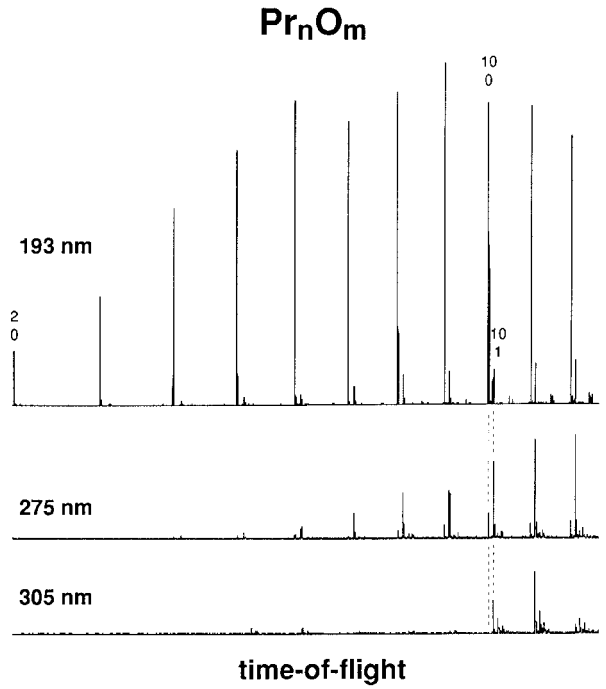

Fig. 1. Time-of-flight mass spectra of Pr_n and Pr_nO_m, recorded at three photoionization laser wavelengths. Mass peaks are labeled according to $\begin{matrix} n \\ m \end{matrix}$.

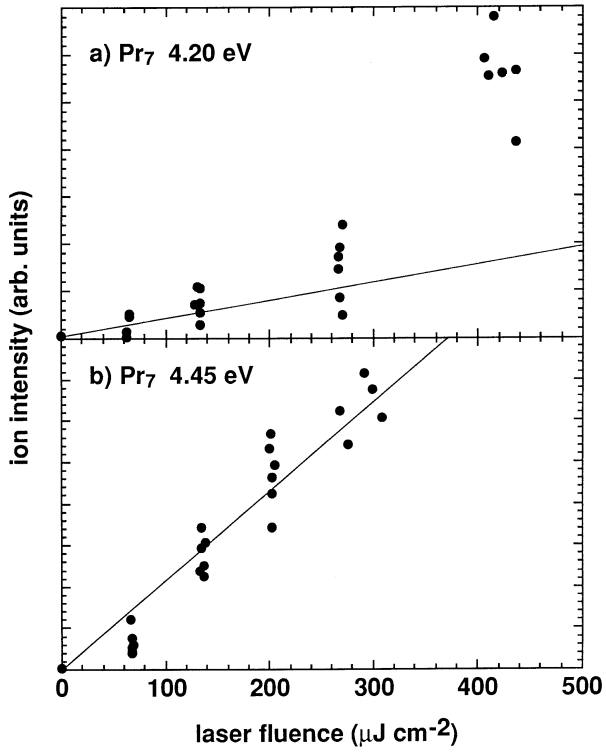

Fig. 2. Ionization signal *vs.* laser fluence for the Pr_7^+ cluster ion signal at: (a) 4.20 eV, below the one-photon IP; (b) 4.45 eV, above the one-photon IP. Lines are drawn for illustrative purposes.

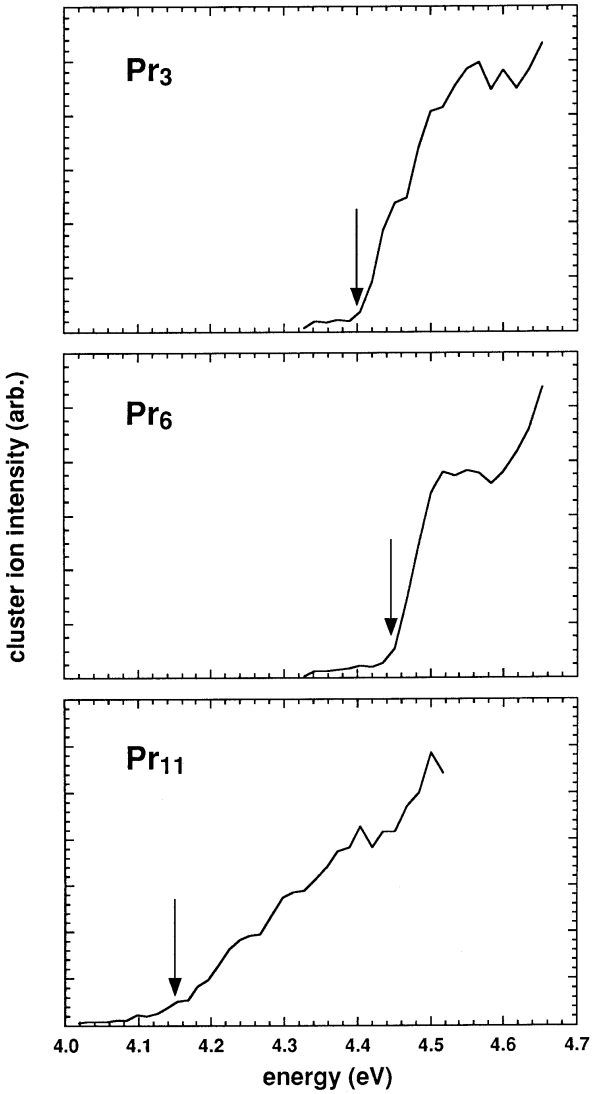

Fig. 3. Photoionization efficiency spectra of Pr_3, Pr_6, and Pr_{11}. The assigned vertical IPs are shown by arrows.

the IPs were generally lowered by ~ 0.1 eV for each oxygen atom in the cluster, as judged from their persistence in the TOF spectra.

When the praseodymium clusters were ionized by an ArF laser operating at fluences greater than those used to determine ionization potentials (*i.e.* fluences in which multiphoton processes competed with single photon processes in producing cluster ion signal), doubly charged clusters as small as Pr_{15}^{2+} were observed. The corresponding doubly charged cluster oxides $Pr_nO_m^{2+}$ ($n \geq 15$, $m = 1$–4) were also observed. As noted above, the fluences used in the PIE and bracketing studies were maintained below 200 μJ cm^{-2}, in which case no doubly charged clusters were observed. Doubly charged lanthanide clusters [9] and lanthanide cluster oxides [10] have been observed previously.

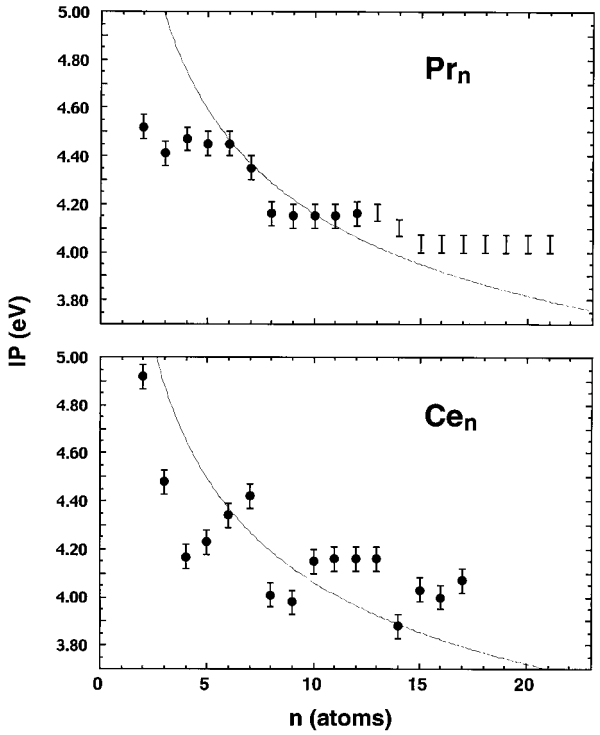

Fig. 4. Vertical ionization potentials of (a) Pr_n and (b) Ce_n. The uncertainty in the assignment of IPs is estimated at 0.05 eV. The solid curves are obtained from equation (2), with $WF_\infty = 2.40$ and 2.50 eV for Ce and Pr, respectively (see text). Note that the WF_∞ value for Ce is somewhat lower than the experimentally measured value (2.9 eV), while the work function of praseodymium has not been experimentally determined.

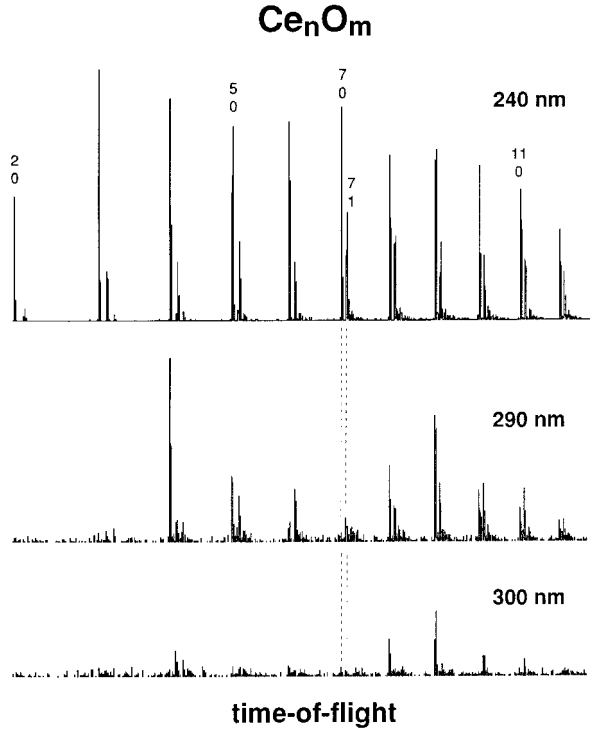

Fig. 5. Time-of-flight mass spectra of Ce_n and Ce_nO_m, recorded at three photoionization laser wavelengths. Mass peaks are labeled according to $\begin{matrix} n \\ m \end{matrix}$.

3.2 Cerium Clusters

Time-of-flight spectra of cerium clusters recorded at different ionization laser wavelengths are shown in Figure 5. PIE spectra for clusters in the size range from Ce_2 to Ce_{17} were obtained in a manner slightly different from that described above for Pr_n clusters. In order to account for large fluctuations in cluster intensity, a second reference TOF spectrum at 193 nm (ArF laser) was recorded on alternate shots. Each normalized TOF peak area obtained with the frequency doubled dye laser was then divided by the corresponding fluence- normalized peak area obtained with the 193 nm laser to give the doubly- normalized ionization cross section $\sigma(\lambda)$:

$$\sigma(\lambda) = [I_\lambda/F_\lambda]/[I_{193}/F_{193}] \quad (1)$$

where I and F are the TOF peak areas and laser fluences, respectively. Representative PIE spectra constructed in this manner at 2.5 nm intervals are displayed in Figure 6. As was done for praseodymium clusters, laser fluence was maintained below 200 μJ cm^{-2} to avoid multiphoton ionization. The vertical ionization potentials for Ce_2–Ce_{17} are shown in Figure 4b. As with the praseodymium clusters, Ce_nO_m clusters were observed to have lower IPs than their Ce_n counterparts, although no explicit measurements of Ce_nO_m PIE spectra were made. Because of the relatively low laser fluence used to determine ionization thresholds, no doubly charged cerium clusters were observed during the course of this study.

The ionization potentials of both the praseodymium and the cerium clusters are tabulated in Table 1.

4 Discussion

The size evolution of the Ce_n and Pr_n IPs is qualitatively similar to that displayed by clusters of transition metal atoms. Specifically, as shown in Figure 2, their IPs vary discontinuously with increasing size, with an overall downward trend toward the work function of the respective solid. The work function of bulk cerium [12] is 2.9 eV, while that of praseodymium has not, to our knowledge, been measured but can be expected to be of a similar value. For ideal metal spheres, a monotonic decrease in IP with increasing radius R is predicted classically by the conducting spherical droplet (CSD) model [13–17]:

$$IP(R) = WF_\infty + e^2/2R \quad (2)$$

where WF_∞ is the work function of the infinite solid, and $e^2/2R$ is the classical charging energy of an ideal finite sphere of radius R. The CSD model, although clearly a gross simplification for molecular objects, is useful in distinguishing the sudden discontinuities in metal cluster IPs reflecting changes in electronic or geometric structure from the slow, monotonic decrease classically predicted with increasing R. The predictions of equation (2)

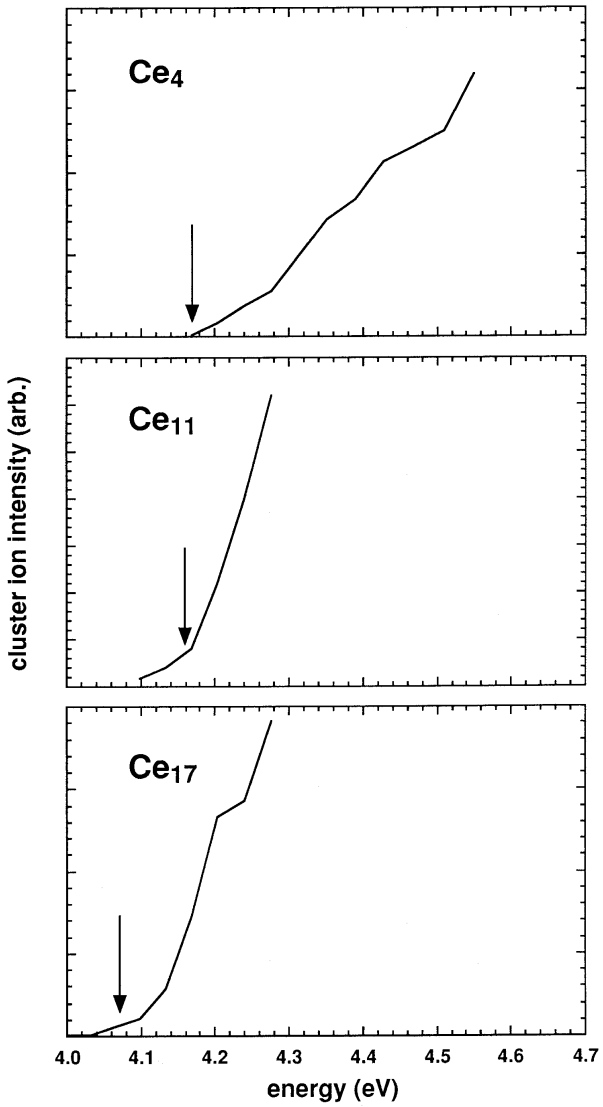

Fig. 6. Photoionization efficiency spectra of Ce_4, Ce_{11}, and Ce_{17}. The assigned vertical IPs are shown by arrows.

are shown along with the experimental data for Ce_n and Pr_n in Figure 4. The discontinuities in the IPs of cerium and praseodymium clusters in the limit of small sizes clearly reflect their molecular nature, behavior which parallels that observed for small transition metal clusters [11, 18–22]. Overall, the IPs of both Ce_n and Pr_n decrease more slowly than the $e^2/2R$ dependence predicted by the CSD model, behavior also typically displayed by transition metal clusters [11,18–22]. A proper description of deviations of IP(R) from the classical prediction as given by equation (2) requires a detailed quantum mechanical treatment [14,15,17].

One of the primary motivations of the present study was to search for evidence of the $4f^36s^2 \rightarrow 4f^2\ (5d,\ 6s)^3$ transition in isolated praseodymium clusters via sudden changes in their photoionization thresholds. As noted in the Introduction, previous searches for evidence of this transition in praseodymium clusters and analogous

Table 1. Vertical ionization potentials for Pr_n and Ce_n clusters. The estimated uncertainty of the assignments is ±0.05 eV.

	IP (eV)	
n	Pr_n	Ce_n
2	4.52	4.92
3	4.41	4.48
4	4.47	4.17
5	4.45	4.23
6	4.45	4.34
7	4.35	4.42
8	4.16	4.01
9	4.15	3.98
10	4.15	4.15
11	4.15	4.16
12	4.16	4.16
13	4.16	4.16
14	4.10	3.88
15	4.04	4.03
16	4.04	4.00
17	4.04	4.07
18	4.04	
19	4.04	
20	4.04	
21	4.04	

$4f^n6s^2 \rightarrow 4f^{n-1}\ (5d,\ 6s)^3$ transitions in other lanthanide metals have been conducted in samples of small particles of these metals that were deposited into rare gas matrices. In the case of praseodymium, the critical particle size, as determined by EXAFS, was estimated to be approximately 5 atoms. The present IP data set for Pr_n clearly includes the previously estimated critical size for the valence transition. As shown in Figure 4a, the IPs of praseodymium clusters display two discontinuities, a 0.3 eV downward step from Pr_6 to Pr_8, and a somewhat smaller step from Pr_{13} to Pr_{15}. With the matrix results discussed above in mind, it is tempting to correlate the larger discontinuity starting at Pr_6 to the valence transition. However, such a correlation is far from definitive. A counterexample is provided by cerium clusters, which, while not expected to undergo a valence transition, display more variation and discontinuity in their IPs than is shown by praseodymium clusters. These results underscore the dominant influence of geometric structure in determining the IPs of small lanthanide clusters. In this sense, Ce_n and Pr_n behave similarly to transition metal clusters, where structures vary discontinuously with size due to the strong influence of localized, directional bonding. The result is a discontinuous evolution of physical properties such as ionization potential. This behavior is in contrast to clusters of nearly-free-electron metals such as sodium and silver, in which the geometric arrangement of the metal ion cores is a less important factor and the size evolution of physical properties mirrors the filling of electronic shells of the delocalized valence electrons. An interpretation of present results would be significantly aided by first-principles electronic structure studies, but would only be meaningful if the approach were capable of accurately treating electron correlation in open-shell, high-Z systems. Density

functional theory is one such approach having both the desired accuracy as well as the computational efficiency necessary for structure optimization.

This work is supported by the U.S. Department of Energy, Office of Basic Energy Sciences, Division of Chemical Sciences, under Contract No. W-31-109-ENG-38.

References

1. L. Brewer, in *Systematics and the Properties of the Lanthanides*, edited by S.P. Sinha (D. Reidel Publishing Company Dordrecht, Holland, 1983) p. 17.
2. J.F. Herbst, Phys. Rev. Lett. **49,** 1586 (1982).
3. W. Niemann, M. Lübcke, W. Malzfeldt, P. Rabe, R. Haensel, J. Magn. and Magn. Mat. **47 & 48,** 462 (1985).
4. M. Lübcke, B. Sonntag, W. Niemann, P. Rabe, Phys. Rev. B **34,** 5184 (1986).
5. W. Niemann, W. Malzfeldt, P. Rabe, R. Haensel, M. Lübcke, Phys. Rev. B **35,** 1099 (1987).
6. C. Blancard, J.M. Esteva, R.C. Karnatak, J.P. Connerade, U. Kuetgens, J. Hormes, J. Phys. B **22,** L575 (1989).
7. M.G. Mason, S.-T. Lee, G. Apai, R.F. Davis, D.A. Shirley, A. Franciosi, J.H. Weaver, Phys. Rev. Lett. **47,** 730 (1981).
8. A. Faeldt, H.P. Myers, J. Magn. and Magn. Mat. **47& 48,** 225 (1985).
9. C. Bréchignac, P. Cahuzac, F. Carlier, M. de Frutos, A. Masson, J.P. Roux, Z. Phys. D **19,** 195 (1991).
10. C. Bréchignac, P. Cahuzac, F. Carlier, J.P. Roux, Z. Phys. D **28,** 67 (1993).
11. M.B. Knickelbein, S. Yang, S.J. Riley, J. Chem. Phys. **93,** 94 (1990).
12. D.E. Eastman, Phys. Rev. B **2,** 1 (1970).
13. G. Makov, A. Nitzan, L.E. Brus, J. Chem. Phys. **88,** 5076 (1988).
14. J.P. Perdew, Phys. Rev. B **37,** 6175 (1988).
15. E. Engel, J.P. Perdew, Phys. Rev. B **43,** 1331 (1991).
16. W.A. de Heer, P. Milani, Phys. Rev. Lett. **65,** 3356 (1990).
17. M. Seidl, K.-H. Meiwes-Broer, M. Brack, J. Chem. Phys. **95,** 1295 (1991).
18. S. Yang, M.B. Knickelbein, J. Chem. Phys. **93,** 1533 (1990).
19. M.B. Knickelbein, S. Yang, J. Chem. Phys. **93,** 5760 (1990).
20. M.B. Knickelbein, J. Chem. Phys. **102,** 1 (1995).
21. G.M. Koretsky, M.B. Knickelbein, J. Chem. Phys. 106 9810 (1997).
22. B.A. Collings, D.M. Rayner, P.A. Hackett, Int. J. Mass Spectrom. Ion Proc. **125,** 207 (1993).